PHILOSOPHICAL TRANSACTIONS A

royalsocietypublishing.org/journal/rsta

Research

Cite this article: Gusakova OV, Galenko PK, Shepelevich VG, Alexandrov DV, Rettenmayr M. 2019 Diffusionless (chemically partitionless) crystallization and subsequent decomposition of supersaturated solid solutions in Sn–Bi eutectic alloy. *Phil. Trans. R. Soc. A* **377**: 20180204.
http://dx.doi.org/10.1098/rsta.2018.0204

Accepted: 20 December 2018

One contribution of 17 to a theme issue 'Heterogeneous materials: metastable and non-ergodic internal structures'.

Subject Areas:
materials science

Keywords:
eutectic structure, rapid solidification, decomposition, grain boundary migration

Authors for correspondence:
Olga V. Gusakova
e-mail: ol.gusakova@gmail.com
Peter K. Galenko
e-mail: peter.galenko@uni-jena.de

Electronic supplementary material is available online at https://dx.doi.org/10.6084/m9.figshare.c.4372448.

Diffusionless (chemically partitionless) crystallization and subsequent decomposition of supersaturated solid solutions in Sn–Bi eutectic alloy

Olga V. Gusakova[1,4], Peter K. Galenko[2], Vasiliy G. Shepelevich[3], Dmitri V. Alexandrov[4] and Markus Rettenmayr[2]

[1]Department of Nuclear and Radiation Safety, International Sakharov Environmental Institute of Belarusian State University, Dolgobrodskaya Street, 23/1, Minsk 220070, Belarus
[2]Department of Physics and Astronomy, Otto Schott Institute for Material Research, Friedrich Schiller University of Jena, Jena 07743, Germany
[3]Department of Solid State Physics, Belarusian State University, Nezavisimosti Avenue, 4, Minsk 220030, Belarus
[4]Department of Theoretical and Mathematical Physics, Laboratory of Multi-Scale Mathematical Modeling, Ural Federal University, Ekaterinburg 620000, Russian Federation

PKG, 0000-0003-2941-7742; DVA, 0000-0002-6628-745X; MR, 0000-0003-4721-5087

Results of a study on microstructural evolution of eutectic Sn-57 wt.% Bi processed with cooling rates of 10^{-2}, $1\,\mathrm{K\,s^{-1}}$ and approximately $10^{5}\,\mathrm{K\,s^{-1}}$ are presented. In order to distinguish different mechanisms of microstructure formation, a comparison with microstructures of different hypoeutectic alloys with compositions down to below the maximum solubility of Bi in Sn–Bi is undertaken. It is found that at the cooling rates of 10^{-2} and $1\,\mathrm{K\,s^{-1}}$, coupled eutectic growth occurs, leading to lamellar structures with different length scales. At the rapid quenching rates of approximately $10^{5}\,\mathrm{K\,s^{-1}}$, structure formation in the eutectic alloy

THE ROYAL SOCIETY PUBLISHING

is qualitatively different. Partitionless solidification resulting in a supersaturated solid solution with the initial composition is observed in both eutectic and hypoeutectic alloys. It is shown that the observed microstructure of the rapidly solidified alloys forms by the decomposition of the supersaturated solid solution.

This article is part of the theme issue 'Heterogeneous materials: metastable and non-ergodic internal structures'.

1. Introduction

Eutectic alloys are known for the complexity of microstructure formation and for their variety of properties [1]. Eutectic alloys are used in several fields in practical applications, e.g. as casting alloys or solder alloys in the electronics industry [2]. Unconventional processing routines are searched for producing solder alloys in forms adapted to the specific application, e.g. with complex shapes by additive manufacturing, or as foils by rapid quenching from the melt. In the latter process, it is essential to control the crystal growth rate, as small variations in the growth undercooling or cooling rate will lead to significant changes in microstructure and properties [3,4].

Sn–Bi alloys have found considerable practical application as Pb-free solders. The influence of the processing conditions on the microstructure of Sn–Bi alloys has been studied by different authors [5–8], where in several works the focus is laid on the influence of the cooling conditions on microstructure formation of eutectic Sn-57 wt.% Bi [9,10]. In these studies, it has been shown that the samples obtained at cooling rates of the order of several 10 s of $\mathrm{K\,s^{-1}}$ exhibit a strongly inhomogeneous microstructure consisting of areas of coarse Bi, areas of irregular eutectic and areas of Sn with fine Bi inclusions.

At low to moderate cooling rates, the microstructure of Sn-57 wt.% Bi forms as regular (lamellar) eutectic; at higher cooling rates, two types of structures with different length scales appear to solidify. Generally, areas with large equiaxed primary Bi crystals and areas with small elongated Bi crystals are detected. In [8], it has been shown that an increase in the cooling rate to $10^3 \ldots 10^5\,\mathrm{K\,s^{-1}}$ leads to a transition from mixed regular + irregular to fully irregular eutectic. To date, the mechanisms of microstructure formation as a function of cooling rate have not been investigated in the available literature, e.g. [7–10].

For low to intermediate cooling rates, solidification occurs close to thermodynamic equilibrium at the solidification front and leads to fine regular eutectic structures that follow expected trends, e.g. a decreasing eutectic colony size and decreasing lamellar spacing for increasing cooling rate. For increasingly higher cooling rates, coupled eutectic growth still prevails, but the regularity of the lamellar structure gradually disappears [7–14]. A further type of microstructure formation occurs at very high cooling rates: the eutectic reaction is suppressed as a result of partitionless solidification [4,15–19].

In [15–18], it was suggested that eutectic reactions in the liquid can be suppressed in the eutectic systems, with the formation of supersaturated solid solutions after solidification. Experimental proofs of this fact with an analysis of the microstructure and composition were obtained in [4,19]. Two studies are available in the literature where eutectic alloys and cooling rates of up to $10^5\,\mathrm{K\,s^{-1}}$ were investigated [4,19]. Conclusions on partitionless solidification of eutectic Al-35%Mg and Pb-11%Sb alloys are drawn, based on the observation of single-phase areas that do not show the typical two-phase eutectic structure. The studies in [4,19] were carried out using optical microscopy with magnifications of up to 1500× and a spatial resolution of approximately 1 µm. However, it is well known that rapid quenching may lead to a substantial refinement of the microstructure [8–13], and the microstructure may consist of finely dispersed inclusions that are not visible in an optical microscope. Thus, the results of the above-mentioned experimental work from the 1980s do not allow us to finally conclude on the formation of a homogeneous solid solution during rapid solidification of eutectic alloys.

In the remarkable work of Boettinger *et al*. [20], the microstructure of Ag–Cu alloys has been investigated upon melting and resolidification at solidification front velocities of 0.01–1.00 m s^{-1}. These authors generated a map of predominant microstructures as a function of solidification velocity and chemical composition. Coupled eutectic growth ceases at 0.02 m s^{-1}, at higher rate first band structures and then microsegregation-free structures at the limit of absolute stability (approx. 0.6 m s^{-1}) appear. The band structure is caused by a reverse behaviour of temperature at the solidification front [21], and the microsegregation-free microstructure appears due to the fact that the partition coefficient approaches unity [22]. This is also confirmed by theoretical considerations [23–25]. The transition to partitionless solidification where solute diffusion does not exert any influence can be defined by the ratio between the solidification front velocity V and the maximum speed of atomic diffusion in the liquid phase V_D [23]: if $V \geq V_D$, the alloy solidifies as a single metastable phase of the initial composition without solute redistribution [24], and the eutectic reaction is suppressed [25]. The latter effect was detected in the very first experiments with rapidly quenched eutectic alloys [15–17]. A systematic experimental study on microstructure formation during rapid solidification of eutectics using up-to-date characterization methods is needed to verify such predictions.

High cooling rates can lead to substantial undercooling before crystallization begins. The influence of undercooling on the character of crystallization of eutectic and hypereutectic alloys of the Sn–Bi system is given in details in [26]. Undercooling by 5–9 K, the eutectic point in the phase diagram shifts towards higher bismuth concentrations. In the eutectic alloy, primary tin is observed, while in the hypereutectic alloys there is no primary bismuth and only eutectic colonies are observed. Thus, it is logical to assume that with the increase in undercooling (achieved with ultrafast quenching), the solidification of the eutectic alloy will proceed not by the mechanism of coupled growth, but by mechanisms specific for hypoeutectic alloys at high cooling rates (partitionless crystallization and the formation of a supersaturated solid solution).

It is pertinent to note that for alloys with relatively low melting temperatures, e.g. Al or lower melting alloys, the microstructure can significantly change after solidification during storage at room temperature, as diffusion or phase transformations may still readily occur. Microstructures of eutectic Sn-57 wt.% Bi are in the present work right after solidification and at later times.

Owing to the thermodynamic state far from equilibrium and the low melting temperature of rapidly solidified eutectic Sn-57 wt.% Bi, further steps in microstructural evolution after solidification may proceed fast and possibly in several stages. The decomposition in Sn–Bi alloys is known to occur by discontinuous precipitation [27] which is characterized by the growth of Bi lamellae in the Sn matrix. Such microstructures have been observed in Sn–Bi alloys for concentrations less than 20 wt.% Bi (i.e. concentrations below the maximum solubility). Previous investigations were devoted to microstructural characterization at temperatures above the solvus temperature (see [27,28] and references therein). A microstructural analysis of quenched and subsequently aged Sn–Bi alloys is, to the best knowledge of the authors, not documented in the literature. The main goal of the present paper is to characterize Sn–Bi microstructures produced under extreme conditions, to understand the mechanism of microstructure formation as a function of cooling rate and to separate the processes of microstructural evolution during solidification and during subsequent solid-state phase transformations.

2. Experimental procedure

Sn–Bi alloys of various compositions (13, 20, 30, 48 and 57 wt.% Bi) were produced by alloying the elements with purity of greater than 99.99% in quartz ampoules. The melt was heated to 550–570 K, as measured by a thermocouple that was placed in the furnace in the vicinity of the ampoules.

The Sn–Bi samples were transferred into a vacuum furnace, heated up again and then rapidly quenched by splashing melt droplets of 0.2–0.3 g on the polished inner surface of a rotating copper chill wheel of 25 cm diameter. The linear velocity at the contact point of the droplets was 15 m s^{-1}.

The thickness of the prepared foils was in the range of 40–80 µm. The cooling rate was of the order of $10^5\,\mathrm{K\,s^{-1}}$, as estimated by calculations [4].

In addition, bulk samples were prepared with a cooling rate of $10^{-2}\,\mathrm{K\,s^{-1}}$ in a resistance muffle furnace (SNOL 0.2/1250). Further samples were solidified in a graphite mould in air atmosphere, their thickness was 3 mm and the cooling rate was approximately $1\,\mathrm{K\,s^{-1}}$.

The samples were polished using Struers TegraPol equipment with water cooling and special cooling suspensions. The final polishing step was carried out with a colloidal silicon suspension, ensuring as little deformation of the surface layer as possible. The microstructures of foils surface, cross-sections and bulk samples were studied in a scanning electron microscope (SEM) LEO 1455 VP using the backscattered electron (BSE) detector.

Grain structure and grain orientation were characterized by electron backscatter diffraction (EBSD) in the SEM, in combination with the phase analysis tool HKL CHANNEL 5.

The chemical composition of the samples was determined by energy-dispersive X-ray spectroscopy (EDX). The constituent phases in the foils were characterized by X-ray diffraction (XRD) using the diffractometer RigakuUltima 4.

Microstructure characterization and determination of the elemental and phase compositions of the rapidly solidified foils were carried out after a series of time intervals. The microstructure at the outer surface was observed 20 min and microstructure in cross-sections was observed 24 h after preparation of foils. SEM and EBSD were employed to monitor post-solidification microstructural evolution (phase transformation and grain boundary migration) *in situ*.

3. Results

Microstructures of the eutectic Sn-57 wt.% Bi samples obtained after solidification at various cooling rates are shown in figure 1. The 'skeleton-like' microstructure (figure 1*a*) is a frequently observed morphology for low cooling rates (of the order of $10^{-2}\,\mathrm{K\,s^{-1}}$). This microstructure consists of eutectic colonies with diameters greater than 100 µm. A colony can be regarded as a conglomerate formed from only one single nucleus of each phase [11]. Coupled growth of the Sn and Bi phases is known to begin with a Bi nucleus which becomes the leading phase and resulting in a regular lamellar microstructure. The mean lamellar spacing in figure 1*a* is 2.3 µm.

A cooling rate of $1\,\mathrm{K\,s^{-1}}$ leads to an irregular eutectic microstructure with varying lamellar spacing (figure 1*b*). In [8], it has been shown that an increase of the cooling rate to $10^3\,\mathrm{K\,s^{-1}}$ leads to the formation of fully irregular eutectic. Our highest cooling rate of approximately $10^5\,\mathrm{K\,s^{-1}}$ leads to a bimodal microstructure (figure 1*c*, different parts designated as 'area A' and 'area B'). A-type areas consist of fine parallel lamellae of Bi and Sn. The mean lamellar spacing and the thickness of the lamellae are approximately 0.1 µm. The extension of areas of A-type is of the order of 6 µm. B-type areas consist of larger globular particles of Bi with a size of approximately 0.5 µm in the Sn matrix. The Bi particles are not arranged regularly. The extension of the areas of B-type is also of the order of 6 µm.

Compositional analysis by EDX reveals that the mean composition in both A-type and B-type areas is the eutectic composition, i.e. Sn-57 wt.% Bi. Micrographs of the cross-sections of foils show similar microstructures as those at the outer surface and at the mould interface, i.e. the two types of A and B structures are observed (figure 2*a*). The chemical composition in transverse sections is uniform, and microsegregation has not been detected (figure 2*b*).

XRD analysis was carried out 1 h after foil production. Reflections corresponding to the solid solution of Bi in Sn and to pure Bi were found. Other phases and compounds were not detected. Figure 3 shows a part of the XRD pattern containing the Sn and Bi lines.

Based on previously published data on the 2θ angle of the 600^1 reflection of the Sn phase that is saturated with Bi (13 wt.% Bi) at the maximum solubility temperature [28] and using the Vegard Law, we estimate the Bi concentration in Sn to be approximately 7 wt.%. This value significantly

[1]Line 600 is a reflection of the 6th order from the crystallographic plane (100) and is located in the high-angle area of the XRD-pattern. Finding of the lattice parameter and concentration of the alloying element by lines located in the high-angle area gives less error, so this line was chosen to analyze the degree of supersaturation of the solid solution.

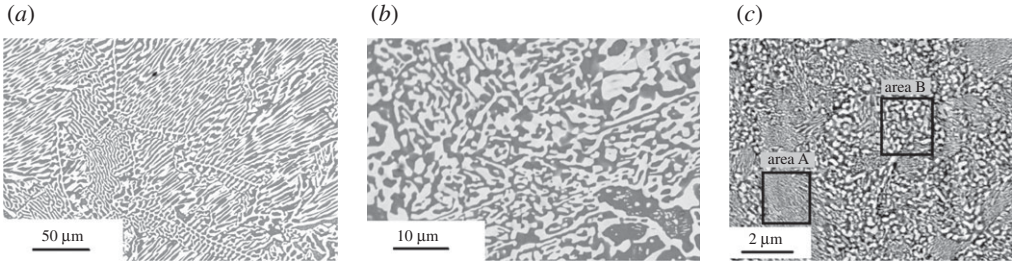

Figure 1. Solidification microstructures of eutectic Sn-57 wt.% Bi samples produced at various cooling rates: 10^{-2} K s^{-1} (*a*), 1 K s^{-1} (*b*) and 10^{5} K s^{-1} (*c*). The white colour corresponds to the Bi phase and the grey colour corresponds to the Sn phase (solid solution of Bi in Sn).

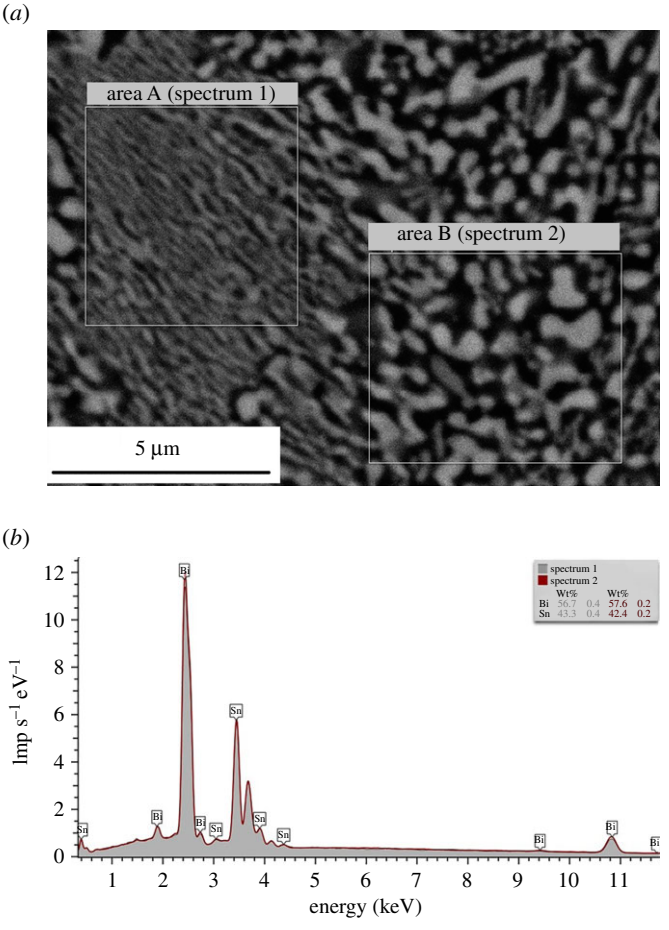

Figure 2. (*a*) Areas with different microstructural types in Sn-57 wt.% Bi foils, obtained at a cooling rate of 10^{5} s^{-1}. (*b*) EDX spectra from areas of A- and B-type. (Online version in colour.)

exceeds the solubility of Bi in Sn at room temperature which is approximately 1.8 wt.% [30]. The Bi reflections in the rapidly solidified foils correspond to pure Bi.

Thus, the increase in the cooling rate from 10^{-2} to 1 K s^{-1} results in a transition from regular to irregular eutectic microstructure. Further increase in the cooling rate up to 10^{5} K s^{-1} results in a second microstructural transition. The presence of two different microstructural types and the high residual Bi concentration in the Sn phase allows us to assume that during rapid solidification

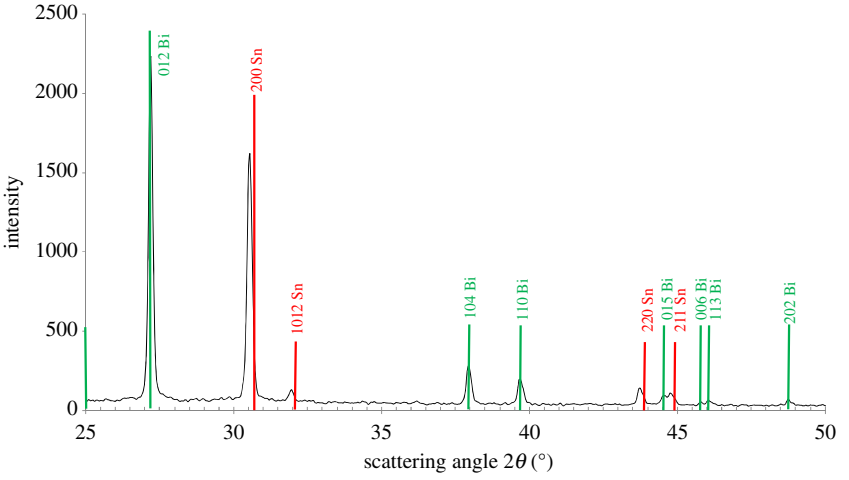

Figure 3. XRD pattern of Sn-57 wt.% Bi foils 1 h after preparation, exhibiting Sn and Bi reflections. Red lines denote the positions of pure Sn, green lines of pure Bi [29].

of eutectic Sn–Bi foils, the eutectic reaction was suppressed. Indeed, there are two different reasons for the high residual concentration in the eutectic Bi–Sn alloy. First, the high residual Bi content can be the result of solute trapping in this phase. Second, during cooling down below the temperature where 7 wt.% Bi is in the Sn phase, cooling kinetics was fast enough to let Bi not diffuse out of Sn. However, the fact that areas of A- and B-type formed by the motion of the decomposition boundary simultaneously with a decrease in residual concentration proofs our assumption about formation of supersaturated solid solution and its subsequent decomposition. In Discussion, we substantiate this suggested assumption.

4. Discussion

The microstructure of the eutectic Sn–Bi obtained at cooling rate $10^{-2}\,\mathrm{K\,s^{-1}}$ corresponds to the regular lamellar microstructure formed by coupled eutectic growth mechanism with the leading phase Bi typical for near-equilibrium solidification [11]. The moderate cooling rate of $1\,\mathrm{K\,s^{-1}}$ leads to a less regular orientation within the eutectic colonies and a decrease in length of the lamellae. Such changes in microstructure may be caused by the presence of convective flow, (soft) impingement of eutectic grains, curvature distribution, etc. In principle, the coupled growth mechanism of the lamellae remains the same.

By contrast, a leading phase and eutectic colonies are not observed in rapidly solidified foils (figure 1*c*). To understand microstructure formation in the foils, we carried out a comparative microstructural analysis of rapidly solidified alloys with Bi concentrations ranging from 13 to 43 wt.%.

Figure 4 presents the equilibrium Sn–Bi phase diagram with arrows marking the compositions investigated in the present work. The samples can be divided into two groups, particularly alloys with nominal concentration (i) below (13 and 20 wt.% Bi) and (ii) above (30, 43 and 57 wt.% Bi) the maximum solubility at 139°C.

(a) Alloys with nominal concentration below maximum solubility

Figure 5 presents microstructures of the Sn-13 wt.% Bi sample after homogenization and quenching; microscopy was carried out after 60 and 120 min. The microstructure changes drastically in the observed time span. The microstructure after 120 min is typical for discontinuous decomposition of a supersaturated solid solution [27]. The process of discontinuous

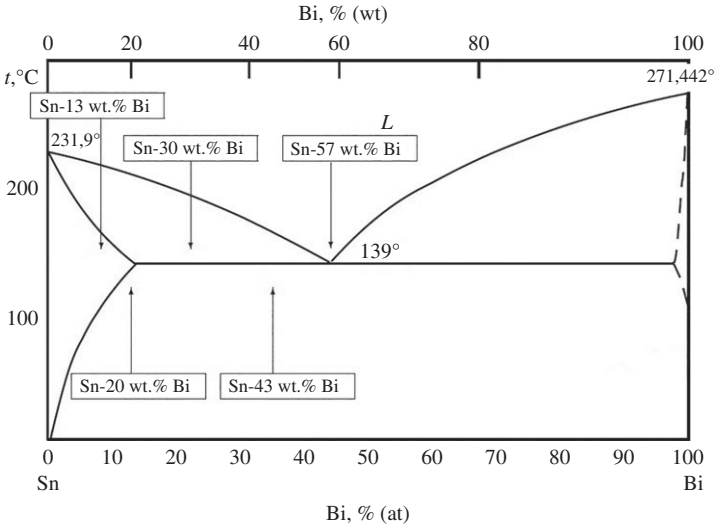

Figure 4. Sn–Bi phase diagram taken from [30].

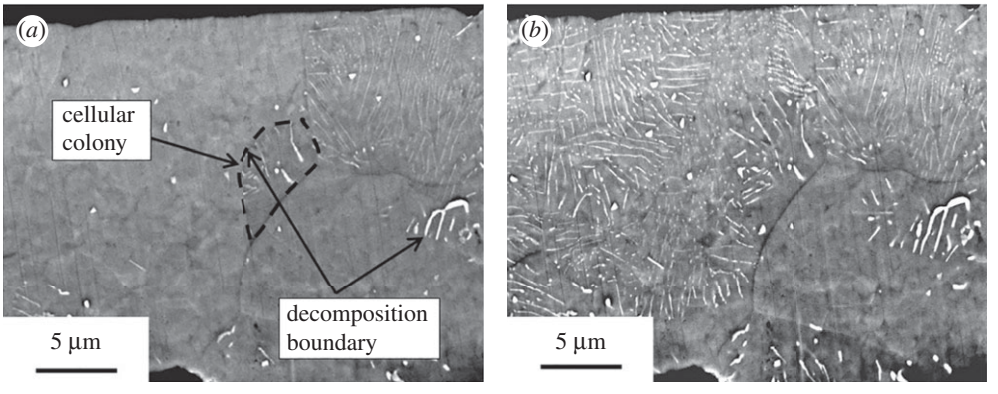

Figure 5. Microstructures of transverse sections of Sn-13 wt.% Bi foils after homogenization and quenching in air at different times after sample homogenization: (*a*) 60 min and (*b*) 120 min.

decomposition begins by an increase in the Bi concentration in the grain boundaries, followed by the formation of new Bi nuclei with lower Sn concentration. The difference in the chemical potentials of Bi and Sn in the grain boundary and the bulk leads to the formation of a transformation front that moves into the bulk, accompanied by an elongation of the Bi nuclei in the direction of the movement. Solute partitioning upon growth yields lamellae arranged in cellular colonies, with a sharp interface between decomposed and undecomposed areas (see arrows in figure 5*a*). EBSD analysis shows that the supersaturated solid solution decomposes by migration of high-angle boundaries (which is characteristic for discontinuous decomposition [27,28,31]).

In the rapidly solidified Sn-13 wt.% Bi alloy, discontinuous decomposition of the solid solution starts 10 min after foil preparation. Figure 6 clearly shows the characteristic microstructural features, i.e. a cellular morphology with Bi lamellae elongated in the direction of the transformation front migration.

The contrast of the Sn phase in the SEM is darker in the decomposed when compared with the undecomposed area. As the micrographs were taken using the BSE detector of the SEM, the darker contrast indicates a lower Bi concentration. EDX analysis also confirmed that the concentration is 13 wt.% Bi in the brighter areas and 8 wt.% Bi in the darker areas. This shows

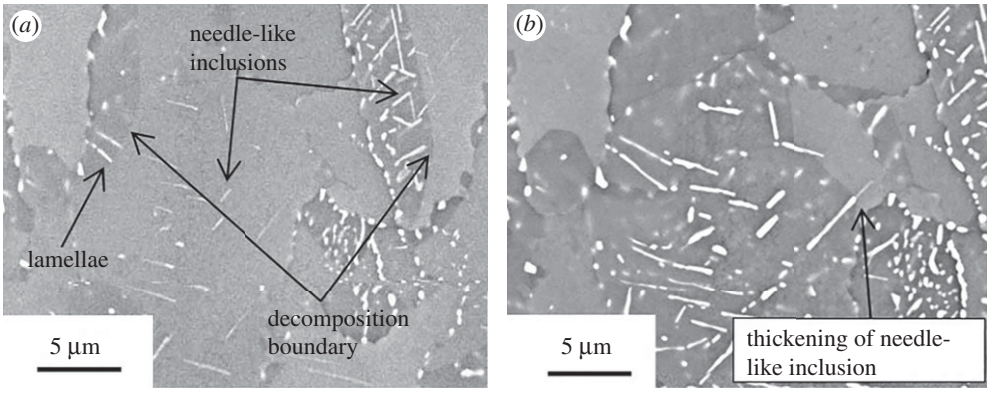

Figure 6. Microstructures at the outer (free) surface of a Sn-13 wt.% Bi foil, observed in (*a*) 25 min and (*b*) 90 min after foil preparation.

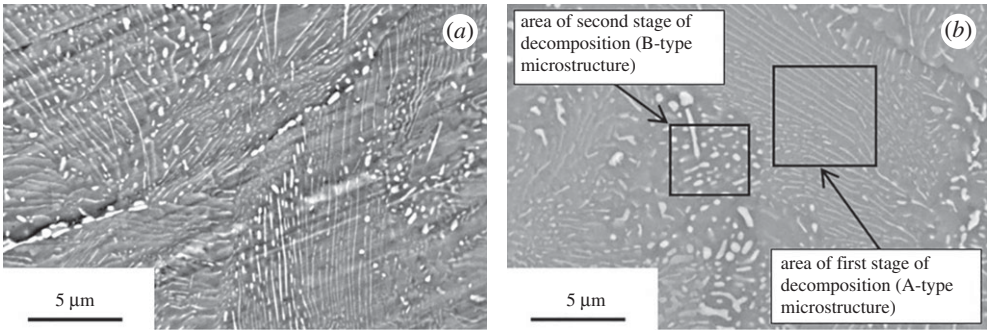

Figure 7. Microstructures of Sn-20 wt.% Bi, 20 min (*a*) and 60 min (*b*) after preparation of the foil.

that the growth of Bi lamellae is sustained by Bi diffusion from the Sn matrix to the precipitates, which leads to further elongation and also thickening of the Bi lamellae.

We also found homogeneously distributed needle-like precipitates that formed by a continuous mechanism (figure 6*a*). They also underwent thickening during decomposition. Discontinuous precipitation does not extend into areas with needle-like precipitates; the needles grow (thicken) with time (figure 6*b*) [28]. The thickness of the continuously precipitated Bi is enhanced by solute atoms segregated in the transformation front that are transported in the vicinity of the continuous precipitates by the discontinuous precipitation [27], accompanied by the faster Bi diffusion along the moving transformation front (see electronic supplementary materials).

The process of decomposition in foils of the Sn-13 wt.% Bi alloy was investigated in the work [28] using XRD analysis. In this work, the coexistence of two Sn 600 lines which correspond to regions with different bismuth concentrations confirms the occurrence of discontinuous decomposition that proceeds with a sharp change of the measured lattice parameter.

This study confirms the high probability of the existence of the presently proposed mechanism of diffusionless (chemically partitionless) crystallization and subsequent decomposition of solid solution in Sn–Bi alloys.

Figure 7 shows microstructures of Sn-20 wt.% Bi (maximum solubility, see phase diagram in figure 4). Twenty minutes after solidification, thin Bi lamellae can be seen in the Sn matrix. The orientation of lamellae is changing from grain to grain. Comparison of the microstructure of Sn-20 wt.% Bi after 20 min (figure 7) with the microstructure of Sn-13 wt.% Bi after 50 min (figures 5 and 6) confirms similar microstructural features, particularly the lamellar microstructure. The

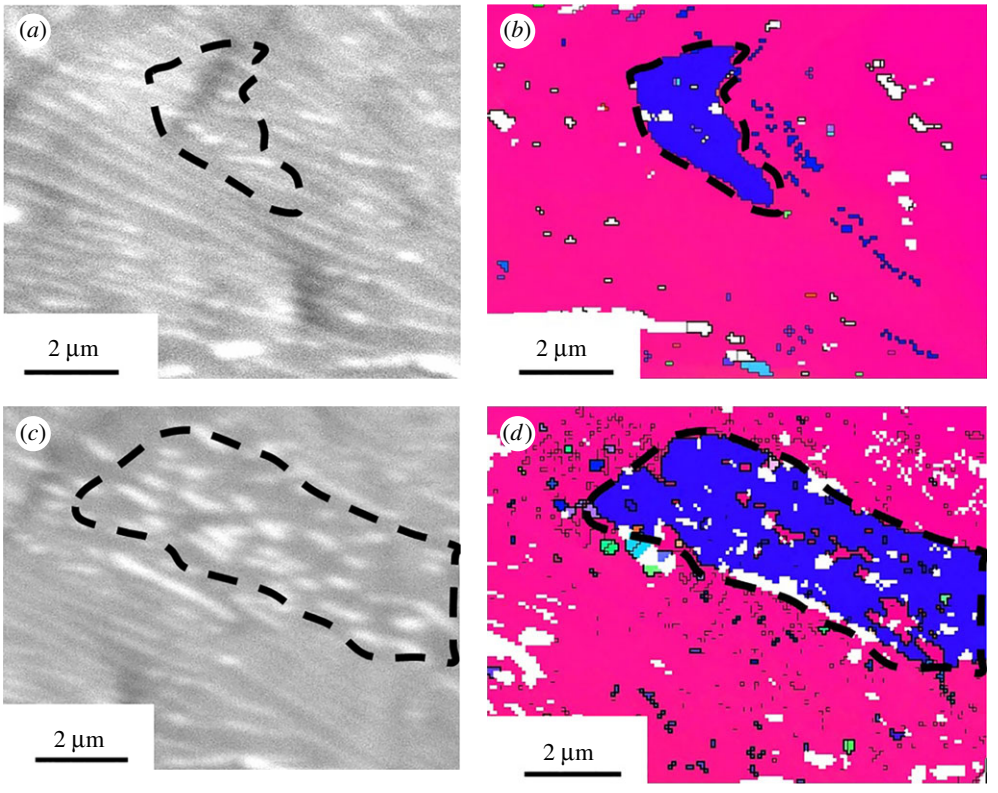

Figure 8. Motion of the boundary of discontinuous decomposition at Sn-20 wt.% Bi: (*a*,*c*) BSE images; (*b*,*d*) EBSD patterns showing misorientations of the Sn phase.

microstructures originate from the same initial microstructure, i.e. a homogeneous supersaturated solid solution that formed by diffusionless solidification during rapid quenching. For both alloys, the decomposition of solid solution proceeded by discontinuous growth. The proceeding transformation front was not observed in the Sn-20 wt.% Bi sample due to the higher bismuth concentration that accelerates the decomposition.

The analysis of further stages of decomposition with time showed that the lamellar structure is unstable at room temperature. Sixty minutes after solidification, the microstructure of Sn-20 wt.% Bi consists of areas with very fine Bi lamellae (see the A-type areas in figure 2*a*) and areas with coarse globular precipitates (see the B-type areas in figure 2*a*). The areas with B-type microstructure are situated near boundaries of the transformation front and clearly separated from the A-type areas. The Sn phase in the B-type areas is distinctly darker, confirming a lower Bi concentration in B-type when compared with A-type areas. This indicates the presence of a second stage of decomposition. The high-angle boundaries of the transformation front move while the size of the Bi precipitates increases due to interface diffusion and with the breaking of Bi lamellae.

In figure 8, results of a study of the same area in the BSE mode of the SEM (figure 8*a*,*c*) and by EBSD (figure 8*b*,*d*) in the Sn-20 wt.% Bi foil are shown. The area was studied twice after a time interval of 30 min (figure 8*c*,*d*). As can be seen in figure 8*b*, two grains are separated by a high-angle boundary (43° of misorientation), with one small grain located inside a larger one. A comparison of this grain structure with the microstructure of figure 8*a* shows that the 'internal' grain is of B-type microstructure and the 'external' grain is of A-type microstructure. After 30 min, the size of the 'internal' grain has increased (figure 8*d*). Simultaneously with the increase in grain size, the area of B-type microstructure grows (figure 8*c*). Thus, we observe the second stage of

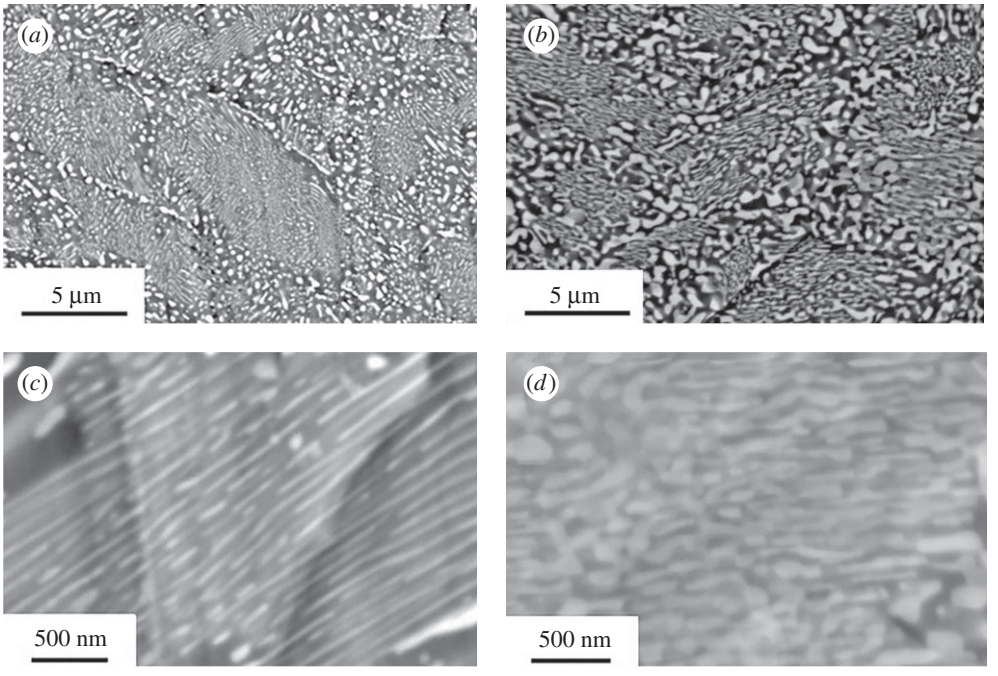

Figure 9. Microstructures of rapidly quenched foils of Sn-30 wt.% Bi (*a*,*c*), Sn-43 wt.% Bi (*b*,*d*).

discontinuous decomposition, similar to in figure 7. The formation of the B-type microstructure is a result of the motion of high-angle decomposition boundaries, as confirmed by EBSD technique.

(b) Hypoeutectic alloys with Bi concentrations above maximum solubility

Foils with Bi concentrations above maximum solubility exhibit similar microstructures as those of the Sn-20 wt.% Bi alloy. Figure 9 shows microstructures of foils of Sn-30 wt.% Bi and Sn-43 wt.% Bi. Again, two types of microstructures are observed: areas of A-type with regular lamellae of Bi (formed during the first stage of decomposition) in Sn, and areas of B-type with coarse equiaxed precipitates (formed during the second stage of decomposition).

An increase in Bi concentration in hypoeutectic Sn–Bi alloys increases the thickness of the lamellae, decreases the lamellar spacing and increases the fraction of coarse equiaxed precipitates. The similarity of these microstructures with those of Sn-20 wt.% Bi allows us to conclude that the solidification has also resulted in a supersaturated solid solution, followed by the discontinuous precipitation in two stages at room temperature. This assumption is confirmed by the fact that the concentration in the microstructures of A- and B-types is equal to the initial (nominal) concentration for all rapidly quenched alloys (cooling rate approx. $10^5\,\mathrm{K\,s^{-1}}$). Hypo- and hypereutectic alloys usually solidify by a dendritic primary phase and interdendritic eutectic. The chemical composition of each structural constituent is, in the near-equilibrium case, the concentration of the respective phase or phase mixture in the equilibrium phase diagram. Thus, the composition of dendrites in hypoeutectic alloys differs distinctly from the nominal concentration. In the present work, rapid quenching led to a uniform concentration distribution, as measured by EDX in areas of $25\,\mu\mathrm{m}^2$.

This confirms

— complete solute trapping of Bi occurs in the Sn matrix during diffusionless primary solidification, forming a supersaturated solution,

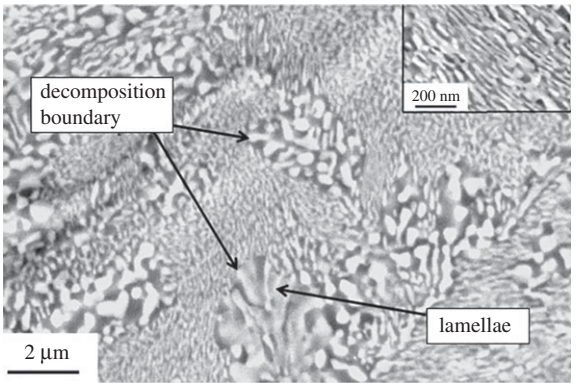

Figure 10. Microstructure of rapidly quenched eutectic Sn-57 wt.% Bi, cooling rate approximately 10^5 K s^{-1}.

— the subsequent discontinuous decomposition at room temperature evolves in two stages,
— bimodal microstructures of A- and B-types are the result of two stages of discontinuous decomposition.

(c) Eutectic composition

As shown in figure 1, the eutectic alloy Sn-57 wt.% Bi also exhibits areas of the two types. In comparison with the hypoeutectic alloys, the microstructure of the eutectic alloy is characterized by the smallest lamellar spacing and the largest extension of B-type areas. Figure 10 exhibits that in some B-type areas, one can find not only relatively large equiaxed Bi precipitates, but also thick lamellae, distinctly thicker than in A-type areas. These findings corroborate the existence of the second stage of discontinuous decomposition. It is concluded that similarly as in hypoeutectic alloys, the decomposition interface of the first stage moves by longitudinal growth of the lamellae, forming cells with lamellar structure.

It is worth noting that in the A-type microstructures, the Bi lamellae are of a smooth shape and a regular spatial distribution. As shown in figure 1*a*,*b*, the increase in the cooling rate from 10^{-2} to 1 K s^{-1} leads to smaller curvature radii of the lamellae and to a loss of the regularity of the eutectic structure. The rapidly quenched microstructures in figures 1*c* and 9 exhibit again regular (or almost regular) structure that is prone to be interpreted as eutectic structure. However, it has been shown in the present work that it is formed by solid-state decomposition. This is further confirmed by an EBSD analysis (figure 11). Differently oriented tin grains are observed with a size greater than or equal to 2 µm. Figure 11*c* shows Bi precipitates with their respective orientation. It can be seen that within a given grain, the Bi precipitates have different orientations. This is not typical for eutectic patterns solidified by a classic coupled growth mechanism. It is clear that the Bi precipitates have nucleated from the solid and not by the eutectic reaction.

Figure 12 shows the results of an ageing study after quenching. Considering the low melting temperature of Sn–Bi, considerable coarsening occurs at room temperature. Figure 12*a* shows the microstructure in 2 h after quenching, displaying areas of both A- and B-type. It appears that the microstructure did not significantly change within 2 h after quenching. After 24 h (figure 12*b*), the volume occupied by B-type areas is significantly increased, while the size of A-type areas decreased from an average linear extension of approximately 6 to 2 µm. We attribute this decrease to the more pronounced ageing at the transformation front of the discontinuous decomposition due to enhanced kinetics at the interfaces. Two hundred hours after quenching (figure 12*c*), the microstructure only consists of B-type microstructure. Further ageing at room temperature (figure 12*b*) leads to the coarsening of the Bi precipitates.

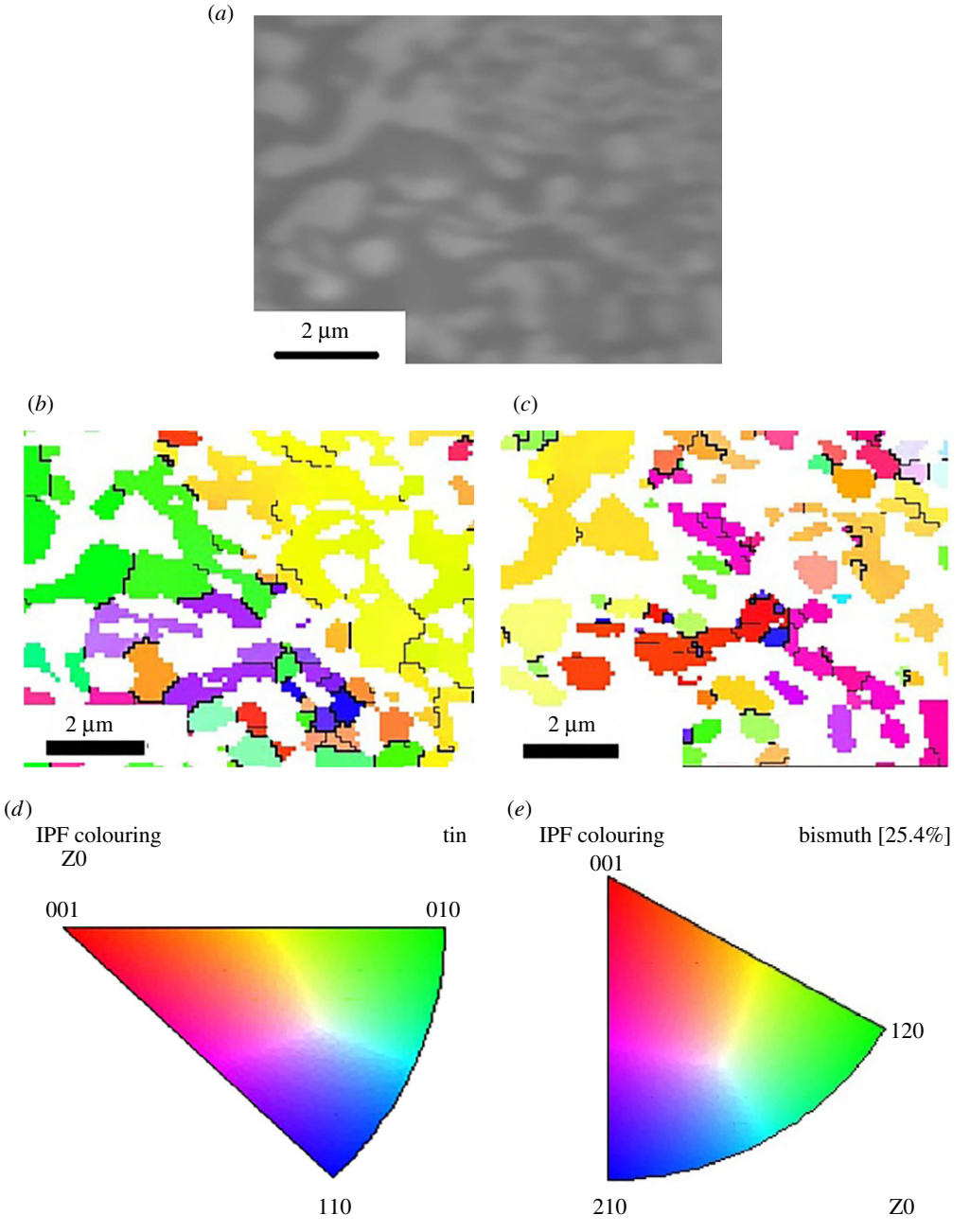

Figure 11. High-resolution EBSC study of a rapidly quenched Sn-57 wt.% Bi alloy. (*a*) SEM microstructure, (*b*,*c*) orientation maps. (*d*,*e*) Sn and Bi colour code of the grain orientation. In (*b*,*c*): Bi is white; thick black lines indicate high-angle boundaries (misorientation $> 15°$); thin black lines show low-angled boundaries (misorientation angle is of 2–5°).

Finally, in order to give an overview for the data of the Sn-57 wt.% Bi eutectic alloy in comparison with other investigated Sn–Bi alloys, table 1 summarizes the times of the first decomposition stage and lamellar spacing at various cooling rates for Sn–Bi alloys. The first stage of decomposition for hypoeutectic and eutectic alloys was very short and not clearly observable in our experiments. It can be seen that the lamellar spacing at cooling rate $10^5\,\mathrm{K\,c^{-1}}$ decreases with the increase in the bismuth concentration.

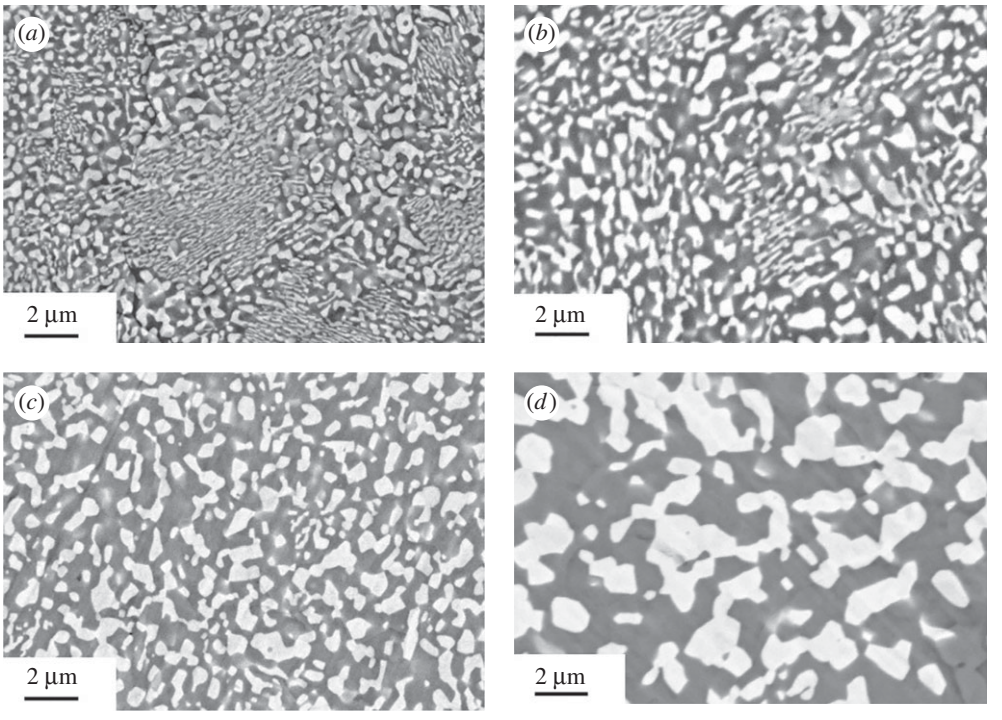

Figure 12. Microstructures of eutectic Sn–Bi after quenching and cold ageing (room temperature) of 2 h (*a*), 24 h (*b*), 200 h (*c*) and 1000 h (*d*).

Table 1. Time of the first stage of decomposition and lamellar spacing depending of concentration of bismuth.

alloy	duration of the first stage of decomposition	lamellar spacing at cooling rate 10^{-2} K c^{-1}	lamellar spacing at cooling rate 10^{5} K c^{-1}
Sn-13 wt.% Bi	4 h	—	0.35 µm
Sn-20 wt.% Bi	20 min	—	0.25 µm
Sn-30 wt.% Bi	<10 min	—	0.12 µm
Sn-58 wt.% Bi	<10 min	3 µm	0.03 µm

5. Conclusion

The effect of the cooling rate on the microstructure of eutectic Sn-57 wt.% Bi has been investigated. Microstructures of this composition were compared with those of hypoeutectic alloys (30 and 43 wt.% Bi) and alloys with nominal concentration below the maximum solubility (13 and 20 wt.% Bi). The following mechanisms of microstructure formation of the Sn–Bi alloy were found:

(i) A eutectic lamellar structure forms by coupled growth at cooling rates of 10^{-2} and 1 K s^{-1}. At 1 K s^{-1}, the Sn and Bi lamellae lose their regularity, become finer and more curved.
(ii) At cooling rates of approximately 10^{5} K s^{-1}, the eutectic reaction is suppressed, and grains of a supersaturated solid solution of Bi in Sn form by partitionless solidification. The chemical composition of the as-solidified Sn grains is the initial (nominal) composition of the melt, qualitatively confirming theoretical predictions [25].
(iii) The rapidly quenched alloy undergoes a decomposition of the supersaturated solid solution at room temperature. For the eutectic alloy, decomposition starts during or

immediately after quenching. Decomposition occurs by discontinuous precipitation. The final microstructure consists of thin regular lamellae of Bi and Sn.

(iv) The formation of the supersaturated solid solution of the eutectic alloy and its subsequent decomposition is confirmed by the following experimental findings:

(a) All rapidly solidified melts exhibit a lamellar structure arranged in cells. The formation of this structure is observed *in situ* for the Sn-13 wt.% Bi alloy.

(b) Grains of the Sn phase contain small and differently oriented precipitates of Bi, in contrast with the eutectic grain structure which is typical for near-equilibrium crystallization and consists of equally oriented lamellae originating from a single nucleus per phase.

(c) The averaged chemical composition of areas with microstructural features of different length scales (areas of A- and B-type, figure 2*a*) always corresponds to the initial composition for the eutectic and hypoeutectic alloys. By contrast, the structure of hypoeutectic alloys after near-equilibrium crystallization consists of grains of the Sn phase with their equilibrium concentration according to the solubility of Bi in Sn, and regions of eutectic composition with a typical eutectic structure.

(d) The formation of areas with coarser microstructures (B-type areas, figure 2*a*) that are a result of a second stage of decomposition is confirmed by the results of ageing treatments resulting in an increase in B-type areas in the whole grain volume and the final microstructure (figure 2*a*).

The description of the mechanisms of formation of the hypoeutectic and eutectic Sn–Bi alloys is of particular interest for the development and testing of a complete theoretical model for microstructure formation including metastable states.

Data accessibility. The data have been uploaded as the electronic supplementary material, movie.

Authors' contributions. All authors contributed equally to the present review paper.

Competing interests. We declare we have no competing interests.

Funding. This work was supported by the German Space Center Space Management under contract no. 50WM1541 (D.V.) and by Russian Science Foundation (project no. 16-11-10095).

Acknowledgements. P.K.G. and M.R. acknowledge support from the German Space Center Space Management under contract no. 50WM1541. D.V.A. acknowledges support of the Russian Science Foundation (project no. 16-11-10095).

References

1. Kurz W, Sahm PR. 1975 *Gerichtet erstarrte eutektische Werkstoffe*. Berlin, Germany: Springer.
2. Lashko SV. 1988 *Soldering of materials*. Moscow, Russia: Mashinostroenie.
3. Gusakova OV, Shepelevich VG. 2010 Structure and properties of quick-hardening foils of alloys of Sn–Zn–Bi system. *Inorg. Mater.: Appl. Res.* **2**, 74–85. (doi:10.1134/S2075113310040143)
4. Miroshnichenko IS. 1982 *Quenching from the liquid state*. Moscow, Russia: Metallurgia.
5. Gusakova OV, Shepelevich VG, Scherbachenk LN. 2014 Effect of melt cooling rate on microstructure of Sn-Bi and Sn-Pb eutectic alloys. *Adv. Mater. Res.* **856**, 236–240. (doi:10.4028/www.scientific.net/AMR.856.236)
6. Li B, Brody HD, Kazimov A. 2004 Real time observation of dendrite coarsening in Sn-13% Bi alloy by synchrotron microradiography. *Phys. Rev. E* **70**, 062602-1–062602-4. (doi:10.1007/s11661-006-9058-5)
7. Yoshioka H, Tada Y, Hayashi Y. 2004 Crystal growth and its morphology in the mushy zone. *Acta Mater.* **52**, 1515–1523. (doi:10.1016/j.actamat.2003.11.033)
8. Zhai QJ, Gao YL, Guan WB, Xu KD. 2006 Role of size and cooling rate in quenched droplet of Sn–Bi eutectic alloy. *Mater. Sci. Eng. A* **441**, 278–281. (doi:10.1016/j.msea.2006.08.050)
9. Hu X, Li K, Ai F. 2012 Research on lamellar structure and micro-hardness of directionally solidified Sn–58Bi eutectic alloy. *China Foundry* **9**, 360–365.

10. Jung H-R, Kim H-H, Lee W-J. 2006 Characterization of small-sized eutectic Sn-Bi solder bumps fabricated using electroplating. *J. Electron. Mater.* **35**, 1067–1073. (doi:10.1007/BF02692568)
11. Taran YN, Mazur VI. 1978 *The structure of eutectic alloys*. Moscow, Russia: Metallurgy.
12. Ojha SN. 2001 Metastable phase formation during solidification of undercooled melt. *Mater. Sci. Eng. A* **304–306**, 114–118. (doi:10.1016/S0921-5093(00)01466-0)
13. Goetzinger R, Barth M, Herlach DM. 1998 Growth of lamellar eutectic dendrites in undercooled melts. *J. Appl. Phys.* **84**, 1643–1649. (doi:10.1063/1.368233)
14. Wei B, Herlach DM, Sommer F. 1993 Rapid eutectic growth of undercooled metallic alloys. *J. Mat. Sci. Lett.* **12**, 1774–1777. (doi:10.1007/BF00517607)
15. Duwez P, Willens RH, Klement W. 1960 Continuous series of metastable solid solutions in silver–copper alloys. *J. Appl. Phys.* **31**, 1136. (doi:10.1063/1.1735777)
16. Jacobson N. 1991 Rapid solidification of Ag-Cu and Ag-Pb alloys. *Mater. Sci. Eng. A* **133**, 574–576. (doi:10.1016/0921-5093(91)90137-C)
17. Sharma SC, Herlach DM. 1992 Salient features of microstructural development in drop-tube processed Al-3.6 wt.% Fe droplets. *Microgravity Sci. Technol.* **3**, 145–150.
18. Walder S, Ryder P. 1993 Critical solidification behavior of undercooled Ag-Cu alloys. *J. Appl. Phys.* **74**, 6100–6106. (doi:10.1063/1.355172)
19. Kucherenko ES, Hluntsev VP. 1989 Rapid crystallization of eutectic alloys. *Metals* **3**, 68–73.
20. Boettinger WJ, Shechtman D, Schaefer RJ, Biancaniello FS. 1984 The effect of rapid solidification velocity on the microstructure of Ag-Cu alloys. *Metal Trans.* **15A**, 55–66. (doi:10.1007/BF02644387)
21. Gremaud MM, Carrard M, Kurz W. 1991 Banding phenomena in Al-Fe alloys subjected to laser surface treatment. *Acta Metall. Mater.* **39**, 1431–1443. (doi:10.1016/0956-7151(91)90228-S)
22. Merchant GJ, Davis SH. 1990 Morphological instability in rapid directional solidification. *Acta Metall. Mater.* **38**, 2683–2693. (doi:10.1016/0956-7151(90)90282-L)
23. Galenko PK, Danilov DA. 1997 Local nonequilibrium effect on rapid dendritic growth in a binary alloy melt. *Phys. Lett. A* **235**, 271–280. (doi:10.1016/S0375-9601(97)00562-8)
24. Galenko PK. 2007 Solute trapping and diffusionless solidification in a binary system. *Phys. Rev. E* **76**, 031606-1–031606-9. (doi:10.1103/PhysRevE.76.031606)
25. Galenko PK, Herlach DM. 2006 Diffusionless crystal growth in rapidly solidifying eutectic systems. *Phys. Rev. Lett.* **96**, 150602-1–150602-4. (doi:10.1103/PhysRevLett.96.150602)
26. Gigliotti MFX, Powell GLF, Colligan GA. 1970 A temperature-composition zone of coupled eutectic growth in the Sn-Bi system. *Metall. Trans.* **1**, 1038–1041.
27. Larikov LN, Shmatko OA. 1976 *Cellular decomposition of supersaturated solid solutions*. Kiev, Ukraine: Naukova dumka.
28. Shepelevich VG, Gusakova OV. 2009 Decomposition of supersaturated solid solution in thin foils of Sn-Bi alloys. *Phys. Met. Metallogr.* **108**, 306–312. (doi:10.1134/S0031918X09090105)
29. ICDD PDF-2 database. 2016. Card : 00-004-0673, Card : 01-085-1329, Quality: S.
30. Lyakishev NP. 1996 *Diagrams of binary metallic systems*. Moscow, Russia: Mechanical Engineering.
31. Zemtsova ND, Starchenko EI. 1980 Possibility of development of cellular decomposition under conditions of low-angled boundary migration. *Fiz. Met. Metalloved.* **50**, 655–659.